SYNTHESIS OF CARBOSILANE DENDRON COATED GOLD NANOPARTICLES AND STUDY OF THEIR POTENTIAL IN PROTEIN SAMPLE PREPARATION

Romy Vásquez-Villanueva[1], Cornelia E. Peña-González[2,3], Rafael Gómez[2,3,4,5], F. Javier de la Mata[2,3,4,5], M. Luisa Marina [1, 3], Javier Sánchez-Nieves[2,3,4,5], M. Concepción García [1, 3*]

[1] Departamento de Química Analítica, Química Física e Ingeniería Química, Universidad de Alcalá, Ctra. Madrid-Barcelona Km. 33.600, 28871 Alcalá de Henares (Madrid), Spain.

[2] Departamento de Química Orgánica y Química Inorgánica, Universidad de Alcalá, Ctra. Madrid-Barcelona Km. 33.600, 28871 Alcalá de Henares (Madrid), Spain.

[3] Instituto de Investigación Química "Andrés M. del Río", Universidad de Alcalá, Ctra. Madrid-Barcelona Km. 33.600, 28871 Alcalá de Henares (Madrid), Spain.

[4] Networking Research Center for Bioengineering, Biomaterials and Nanomedicine (CIBER-BBN), Málaga, Spain

[5] Institute Ramón y Cajal for Health Research (IRYCIS)

*Corresponding author (e-mail: concepcion.garcia@uah.es, telephone +34-918854915; fax +34-918854971)

Abstract

This work evaluates the feasibility of carbosilane dendronized gold nanoparticles (GNPs) in protein sample preparation. Three different dendrons (sulfonate terminated (STC-GNP), carboxylate terminated (CTC-GNP), and trimethylammonium terminated (ATC-GNP) with three different generations (1G, 2G, and 3G) were employed. Moreover, a method for the synthesis of CTC-GNP was proposed from new carboxylate dendrons, whilst the other two dendronized GNPs were synthetized using previously described routes. Three different standard proteins were employed to study the potential of GNPs to interact with proteins. Studies were based on the monitorization of intrinsic fluorescence intensity of proteins and their maximum emission wavelength. Most favoring dendrons for the interaction with standard proteins were anionic carboxylate and sulfonate-terminated under acid and neutral conditions. These conditions and GNPs promoted the establishment of electrostatic interactions with positively charged proteins. Finally, dendronized GNPs were applied to the extraction of proteins from a complex sample, a peach seed, as a cleaner alternative to traditional extraction methods using organic and polluting reagents.

Keywords: carbosilane dendron, gold nanoparticle, protein-gold nanoparticle interaction, protein extraction

1. Introduction

The development of nanotechnology has enabled the development of new materials that have been applied for different purposes. Special attention have received metal nanoparticles, specifically gold nanoparticles (GNP,) due to their optical properties, high stability, large surface-volume ratio, biocompatibility, inertness, and low toxicity. Moreover, their synthesis usually requires the use of green routes [1, 2].

One of the most attractive features of GNPs is their easy functionalization (commonly by using Brust–Schiffrin method) resulting in an enhanced stability and a more controlled size [3]. Functionalization of GNPs was initially used to prevent their aggregation. Nevertheless, GNPs functionalization can dramatically modify their surface properties and applications. The use of dendrimers as covering agents has led to more stable GNPs than those observed with other usual functional groups [4, 5]. Dendrimers are macromolecules with globular structure, a well-established size, and a structure made up of a central core (zero generation) with branches called dendrons. Moreover, dendrons, with a conical shape, can be functionalized by groups or ligands that make them suitable for the interaction with biological molecules [6, 7]. One of the most focused dendrimer in literature has been hydrophilic polyamidoamine, also known as PAMAM. Nevertheless, different works has also reported PAMAM toxicity [8-10]. Another kind of dendrimer are carbosilane ones characterized by their hydrophobic C-Si backbone, easy functionalization, and chemical and biological stability [11]. Carbosilane dendrimers present a significantly lower toxicity than PAMAM and have showed capability to interact with biomolecules such as proteins [8, 12, 13]. This interaction can also being favoured by the presence of the hydrophobic carbosilane framework [Sánchez-Milla, M.; Pastor, I.; Maly, M.; Serramía, M. J.; Gómez, R.; Sánchez-Nieves, J.; Ritort, F.; Muñoz-Fernández, M. Á.; de la Mata, F. J. Study of non-

covalent interactions on dendriplex formation: influence of hydrophobic, electrostatic and hydrogen bonds interactions. *Colloids Surf. B: Biointerfaces* **2018**, *162*, 380-388]. Indeed, recent studies demonstrated the feasibility of anionic carbosilane dendrimers (suphonate and carboxilate) of different generations to interact with proteins under different pH conditions [14, 15]. Moreover, these interactions led to their application in the extraction and purification of proteins from complex matrices. Successful results were also obtained when applying dendrimer coated single walled carbon nanotubes in protein sample preparation [16]. On the other hand, a recent study with GNPs coated with cationic carbosilane dendrons showed its interaction with serum human albumin, preferably at basic pH [17]. Moreover, different studies have demonstrated that proteins can interact with nanoparticles through different forces (electrostatic forces, dispersive and solvation forces, hydrogen bonds, Van der Waals forces, and covalent interactions) and that these interactions are highly depended on protein conformation and charge [18-20].

Synthesis of sulfonate and trimethylammonium terminated carbosilane dendron coated GNPs has been carried out through the reduction of a gold derivative in the presence of dendrons with a thiol moiety at the focal point. These GNPs showed amazing antibacterial, antifungal, and antiviral activity (inhibiting HIV-1 infection) that enabled their application for biomedical purposes [21, 22]. The aim of this work was to study the feasibility of sulfonate and trimethylammonium terminated carbosilane dendrons coated GNPs in protein sample preparation. Additionally, previous results of our research group reveled the potential of carboxylate terminated carbosilane dendrimers in protein sample preparation [15]. This work also purposes the synthesis of carboxylate terminated carbosilane dendron coated GNPs and the evaluation of their potential in the extraction of proteins.

2. Experimental part

2.1. General Considerations

Reactions were carried out under inert atmosphere. Solvents were purified with MBraun-SPS purification system and storage into ampoules containing molecular sieves. NMR spectra were recorded on a Varian Unity VXR-300 (300.13 (^{1}H), 75.47 (^{13}C) MHz) or on a Bruker AV400 (400.13 (^{1}H), 100.60 (^{13}C), 79.49 (^{29}Si) MHz). Chemical shifts (δ) are given in ppm. ^{1}H and ^{13}C resonances were measured relative to solvent peaks considering TMS = 0 ppm, meanwhile ^{29}Si resonances were measured relative to external tetramethylsilane. When necessary, assignment of resonances was done from HSQC, HMBC, COSY and TOCSY NMR experiments.

2.2. Reagents

Water was obtained from a Milli-Q system from Millipore (Bedford, MA, USA). Bovine serum albumin (BSA), chicken egg white lysozyme (Lyz), equine heart myoglobin (Myo), dithiothreitol (DTT), β-mercaptoethanol, trifluoroacetic acid (TFA), 2,2'-dimethoxy-2-phenylacetophenone (DMPA), $NaAuCl_4$ and $NaBH_4$ were purchased from Sigma-Aldrich (Saint Louis, MO, USA). Tris(hydroxymethyl)aminomethane (Tris), sodium dodecyl sulphate (SDS) and hydrochloric acid (HCl) were from Merck (Darmstadt, Germany). Acetone, hexane, methanol (MeOH), ethanol, and acetic acid (AA) were from Scharlau Chemie (Barcelona, Spain). $HS(CH_2)CO_2Me$ were obtained for Acros. Dendrons $MeCOSG_nV_m$ were prepared as previously reported [E. Fuentes-Paniagua, C. E. Peña-González, Marta Galán, R. Gómez, F. J. de la Mata, J. Sánchez-Nieves, Thiol-Ene Synthesis of Cationic Carbosilane Dendrons: a New Family of Synthons. *Organometallics* **2013**, *32*, 1789−1796]. Mini-Protean precast gels, Laemmli buffer, Tris/Glycine/SDS running buffer, Precision Plus Protein Standard (containing highly purified recombinant proteins with MWs from 10 to 250 kDa), Bio-Safe™

Coomassie stain, Silver Stain Plus™ kit, and Bradford reagent (Coomassie (Brilliant) Blue G-250 dye) were obtained from Bio-Rad (Hercules, CA, USA).

2.3. Methods

2.3.1. Dendron synthesis

(MeCOS)G$_1$(S-CO$_2$Me)$_2$ (**1**). A THF solution of HS(CH$_2$)CO$_2$Me (6.58 g, 17.44 mmol) was added to a THF solution of precursor dendron MeCOSG$_1$V$_2$ (1.94 g, 8.51 mmol) in the presence of DMPA (10%) as catalyst and the mixture was stirred under ultraviolet light (hν) for 4 h. Volatiles were removed under vacuum and residues were purified by size-exclusion chromatography using THF as eluent, affording **1** as orange oil (1.19 g, 70 %). Data for **1**: $C_{17}H_{32}O_5S_3Si$ (440.70 g.mol^{-1}). **NMR (CDCl$_3$): ^{1}H**: δ 0.01 (s, 3 H, SiC*H$_3$*), 0.55 (m, 2 H, SCH$_2$CH$_2$CH$_2$C*H$_2$*Si), 0.88 (m, 4 H, SiC*H$_2$*CH$_2$S), 1.32 (m, 2 H, SCH$_2$CH$_2$C*H$_2$*CH$_2$Si), 1.56 (m, 2 H, SCH$_2$C*H$_2$*CH$_2$CH$_2$Si), 2.30 (s, 3 H, C*H$_3$*COS), 2.63 (m, 4 H, SiCH$_2$C*H$_2$*S), 2.84 (t, J = 7.3 Hz, 2 H, SC*H$_2$*CH$_2$CH$_2$CH$_2$Si), 3.22 (s, 4 H, SC*H$_2$*CO$_2$), 3.71 (s, 6 H, CO$_2$C*H$_3$*); **^{13}C{^{1}H}**: δ -5.4 (Si*C*H$_3$), 13.0 (SCH$_2$CH$_2$CH$_2$*C*H$_2$Si), 13.8 (Si*C*H$_2$CH$_2$S), 22.8 (SCH$_2$CH$_2$*C*H$_2$CH$_2$Si), 28.1 (SiCH$_2$*C*H$_2$S), 28.6 (S*C*H$_2$CH$_2$CH$_2$CH$_2$Si), 30.7 (*C*H$_3$COS), 33.1 (SCH$_2$*C*H$_2$CH$_2$CH$_2$Si), 33.3 (S*C*H$_2$CO$_2$), 52.4 (CO$_2$*C*H$_3$), 171.0 (*C*O$_2$CH$_3$) 196.0 (CH$_3$*C*OS); **{^{1}H-^{29}Si}**: δ 2.4 (*Si*CH$_3$). **MS:** [M + H]$^+$: 441.12, [M + NH$_4$]$^+$: 458.15, [M + Na]$^+$: 463.11. **Elemental Analysis:** Calcd.: C, 46.33; H, 7.32; S, 21.82; Obt.: C, 47.57; H, 7.51; S, 21.65.

(MeCOS)G$_2$(S-CO$_2$Me)$_4$ (**2**). Following the procedure described for compound **1**, compound **2** was obtained (1.82 g, 56 %) as orange oil from the reaction of HS(CH$_2$)CO$_2$Me (5.69 g, 15.08 mmol) with precursor dendron MeCOSG$_2$V$_4$ (1.69 g, 3.72 mmol). Data for **2**: $C_{35}H_{68}O_9S_5Si_3$ (876.28 g.mol^{-1}). **NMR (CDCl$_3$): ^{1}H**: δ -0.13 (s, 3 H, SiC*H$_3$*), -0.03 (s, 6 H, SiC*H$_3$*), 0.48 (m, 10 H, SCH$_2$CH$_2$CH$_2$C*H$_2$*Si, SiC*H$_2$*CH$_2$C*H$_2$*Si), 0.84 (m, 8 H, SiC*H$_2$*CH$_2$S), 1.25 (m, 6 H, SCH$_2$CH$_2$C*H$_2$*CH$_2$Si, SiCH$_2$C*H$_2$*CH$_2$Si), 1.52 (m, 2 H, SCH$_2$C*H$_2$*CH$_2$CH$_2$Si), 2.26 (s, 3 H, C*H$_3$*COS), 2.60 (m, 8 H, SiCH$_2$C*H$_2$*S), 2.80 (t, J = 7.3 Hz, 2 H, SC*H$_2$*CH$_2$CH$_2$CH$_2$Si), 3.18 (s, 8 H, SC*H$_2$*CO$_2$), 3.67 (s, 12 H, CO$_2$C*H$_3$*); **^{13}C{^{1}H}**: δ -5.5 (1 Si*C*H$_3$), -5.3 (2 Si*C*H$_3$), 13.2 (SCH$_2$CH$_2$CH$_2$*C*H$_2$Si), 13.9 (Si*C*H$_2$CH$_2$S), 18.1, 18.2, 18.5 (Si*C*H$_2$*C*H$_2$*C*H$_2$Si), 23.1 (SCH$_2$CH$_2$*C*H$_2$CH$_2$Si), 28.1 (SiCH$_2$*C*H$_2$S), 28.6 (S*C*H$_2$CH$_2$CH$_2$CH$_2$Si), 30.5 (*C*H$_3$COS), 33.1 (SCH$_2$*C*H$_2$CH$_2$CH$_2$Si, S*C*H$_2$CO$_2$), 52.2 (CO$_2$*C*H$_3$), 170.8 (*C*O$_2$CH$_3$) 195.8 (CH$_3$*C*OS); **{^{1}H-^{29}Si}**: δ 1.7 (1 *Si*CH$_3$), 2.4 (2 *Si*CH$_3$). **MS:** [M + NH$_4$]$^+$: 894.31. **Elemental Analysis:** Calcd.: C, 47.91; H, 7.81; S, 18.27; Obt.: C, 47.93; H, 7.66; S, 18.19.

(MeCOS)G$_3$(S-CO$_2$Me)$_8$ (**3**). Following the procedure described for compound **1**, compound **3** was obtained (1.65 g, 56 %) as orange oil from the reaction of HS(CH$_2$)CO$_2$Me (5.38 g, 14.25 mmol) with precursor dendron MeCOSG$_3$V8$_4$ (1.52 g, 1.69 mmol). Data for **3**: $C_{71}H_{140}O_{17}S_9Si_7$ (1751.02 g.mol^{-1}). **NMR (CDCl$_3$): ^{1}H**: δ -0.11 (s, 9 H, SiC*H$_3$*), -0.001 (s, 12 H, SiC*H$_3$*), 0.51 (m, 26 H, SCH$_2$CH$_2$CH$_2$C*H$_2$*Si, SiC*H$_2$*CH$_2$C*H$_2$*Si), 0.87 (m, 16 H, SiC*H$_2$*CH$_2$S), 1.28 (m, 14 H, SCH$_2$CH$_2$C*H$_2$*CH$_2$Si, SiCH$_2$C*H$_2$*CH$_2$Si), 1.55 (m, 2 H, SCH$_2$C*H$_2$*CH$_2$CH$_2$Si), 2.28 (s, 3 H, C*H$_3$*COS), 2.63 (m, 16 H, SiCH$_2$C*H$_2$*S), 2.83 (m, 2 H, SC*H$_2$*CH$_2$CH$_2$CH$_2$Si),

3.21 (s, 16 H, SC*H*$_2$CO$_2$), 3.70 (s, 24 H, CO$_2$C*H*$_3$); **^{13}C{^{1}H}**: δ -5.3 (3 Si*C*H$_3$), -5.0 (4 Si*C*H$_3$), 13.4 (SCH$_2$CH$_2$CH$_2$*C*H$_2$Si), 14.0 (Si*C*H$_2$CH$_2$S), 18.3, 18.4, 18.9 (SiC*H*$_2$*C*H$_2$*C*H$_2$Si), 23.4 (SCH$_2$CH$_2$*C*H$_2$CH$_2$Si), 28.2 (SiCH$_2$*C*H$_2$S), 28.8 (S*C*H$_2$CH$_2$CH$_2$CH$_2$Si), 30.7 (*C*H$_3$COS), 33.2 (SCH$_2$*C*H$_2$CH$_2$CH$_2$Si, S*C*H$_2$CO$_2$), 52.4 (CO$_2$*C*H$_3$), 171.0 (*C*O$_2$CH$_3$) 196.0 (CH$_3$*C*OS); **{^{1}H-^{29}Si}**: δ 0.8 (3 *Si*CH$_3$), 2.4 (4 *Si*CH$_3$). **MS:** [M + 2H]$^{2+}$: 876.30, [M + 2 H$_2$O]$^{2+}$: 893.31, [M + H$_2$O]$^+$: 1768.62. **Elemental Analysis:** Calcd.: C, 48.70; H, 8.06; S, 16.48; Obt.: C, 47.90; H, 7.09; S, 16.06.

HSG$_1$(S-CO$_2$H)$_2$ (4). Compound **1** (1.86 g, 4.23 mmol) were suspended in a mixture of NaOH (761.4 mmol, aqueous solution, 60 eq. per group to deprotect) and THF (v/v = 1:2). The suspension was stirred at 45 ºC for 24 hours. Afterwards, THF was evaporated and the residue was washed with CH$_2$Cl$_2$ (5 mL x 3 times). The residue was dissolved in water and hydrochloric acid (4 M) was added until a viscous precipitate was formed. The water was decanted and the viscous precipitate was washed with water (5 mL x 3 times) affording **4** as orange oil (1.44 g, 93 %). Data for **4**: C$_{13}$H$_{26}$O$_4$S$_3$Si (370.61 g.mol^{-1}). **NMR (CD$_3$OD): ^{1}H**: δ 0.07 (s, 3 H, SiC*H*$_3$), 0.62 (m, 2 H, SCH$_2$CH$_2$CH$_2$C*H*$_2$Si), 0.96 (m, 4 H, SiC*H*$_2$CH$_2$S), 1.38 (m, 1 H, S*H*), 1.48 (m, 2 H, SCH$_2$CH$_2$C*H*$_2$CH$_2$Si), 1.65 (m, 2 H, SCH$_2$C*H*$_2$CH$_2$CH$_2$Si), 2.53 (m, 2 H, SC*H*$_2$CH$_2$CH$_2$CH$_2$Si), 2.73 (m, 4H, SiCH$_2$C*H*$_2$S), 3.25 (s, 4 H, SC*H*$_2$COOH), not observed (s, 2 H, COO*H*); **^{13}C{^{1}H}**: δ -5.2 (Si*C*H$_3$), 13.8 (SCH$_2$CH$_2$CH$_2$*C*H$_2$Si), 14.8 (Si*C*H$_2$CH$_2$S), 23.4 (SCH$_2$CH$_2$*C*H$_2$CH$_2$Si), 24.5 (S*C*H$_2$CH$_2$CH$_2$CH$_2$Si) 28.8 (SiCH$_2$*C*H$_2$S), 34.0 (*C*H$_2$COOH), 38.8 (SCH$_2$*C*H$_2$CH$_2$CH$_2$Si), 174.4 (*C*OOH); **{^{1}H-^{29}Si}**: δ 2.5 (*Si*CH$_3$). **MS:** [M + Na]$^+$: 393, [M - H + Na + NH$_4$]$^+$: 410, [M - 2 H + Na + 2 NH$_4$]$^+$: 427. **Elemental Analysis:** Calcd.: C, 42.13; H, 7.07; S, 25.95; Obt.: C, 43.26; H, 8.62; S, 27.59.

HSG$_2$(S-CO$_2$H)$_4$ (5). Following the procedure described for compound **4**, compound **5** was obtained (0.52 g, 90 %) as orange oil from the reaction of **2** (0.65 g, 0.74 mmol) with NaOH (222 mmol). Data for **5**: C$_{29}$H$_{58}$O$_8$S$_5$Si$_3$ (779.35 g.mol^{-1}). **NMR (CD$_3$OD): ^{1}H**: δ -0.02 (s, 3 H, SiC*H*$_3$), 0.07 (s, 6 H, SiC*H*$_3$), 0.68 (m, 10 H, SCH$_2$CH$_2$CH$_2$C*H*$_2$Si, SiC*H*$_2$CH$_2$C*H*$_2$Si), 0.97 (m, 8 H, SiC*H*$_2$CH$_2$S), 1.45 (m, 7 H, SCH$_2$CH$_2$C*H*$_2$CH$_2$Si, SiCH$_2$C*H*$_2$CH$_2$Si, *H*S), 1.64 (m, 2 H, SCH$_2$C*H*$_2$CH$_2$CH$_2$Si), 2.53 (m, 2 H, SC*H*$_2$CH$_2$CH$_2$CH$_2$Si), 2.73 (m, 8 H, SiCH$_2$C*H*$_2$S), 3.26 (s, 8 H, SC*H*$_2$COOH), not observed (s, 2 H, COO*H*);**^{13}C{^{1}H}**: δ -4.9 (1 Si*C*H$_3$), -4.6 (2 Si*C*H$_3$), 14.5 (SCH$_2$CH$_2$CH$_2$*C*H$_2$Si), 15.1 (Si*C*H$_2$CH$_2$S), 19.3, 19.6 (Si*C*H$_2$*C*H$_2$*C*H$_2$Si), 23.8 (SCH$_2$CH$_2$*C*H$_2$CH$_2$Si), 24.6 (S*C*H$_2$CH$_2$CH$_2$CH$_2$Si) 28.9 (SiCH$_2$*C*H$_2$S), 34.3 (*C*H$_2$COOH), 39.5 (SCH$_2$*C*H$_2$CH$_2$CH$_2$Si), 174.5 (*C*OOH); **{^{1}H-^{29}Si}**: δ 1.6 (1 *Si*CH$_3$), 2.5 (2 *Si*CH$_3$). **MS:** [M + Na]$^+$: 801.00, [M - H + 2 Na]$^+$: 823.00. **Elemental Analysis:** Calcd.: C, 44.69; H, 7.50; S, 20.57; Obt.: C, 44.14; H, 7.90; S, 21.18.

HSG$_3$(S-CO$_2$H)$_8$ (6). Following the procedure described for compound **4**, compound **6** was obtained (0.52 g, 90 %) as orange oil from the reaction of **3** (0.86 g, 0.49 mmol) with NaOH (264.6 mmol). Data for **6**: C$_{261}$H$_{122}$O$_{16}$S$_9$Si$_7$ (1594.46 g.mol^{-1}). **NMR (CD$_3$OD): ^{1}H**: δ -0.01 (s, 9 H, SiC*H*$_3$), 0.07 (s, 12 H, SiC*H*$_3$), 0.64 (m, 26 H, SCH$_2$CH$_2$CH$_2$C*H*$_2$Si, SiC*H*$_2$CH$_2$C*H*$_2$Si), 0.96 (m, 16 H, SiC*H*$_2$CH$_2$S), 1.41 (m, 16 H, SCH$_2$CH$_2$C*H*$_2$CH$_2$Si, SiCH$_2$C*H*$_2$CH$_2$Si, SCH$_2$C*H*$_2$CH$_2$CH$_2$Si), 2.72 (m, 10 H, SC*H*$_2$CH$_2$CH$_2$CH$_2$Si, SiCH$_2$C*H*$_2$S), 3.25 (s, 16 H, SC*H*$_2$COOH), not observed (s, 2 H, COO*H*);**^{13}C{^{1}H}**: δ -4.7 (3 Si*C*H$_3$), -4.5 (4 Si*C*H$_3$), 14.3

($SCH_2CH_2CH_2CH_2Si$, $SiCH_2CH_2S$), 19.5, 19.7, 19.9 ($SiCH_2CH_2CH_2Si$), 23.9 ($SCH_2CH_2CH_2CH_2Si$, $SCH_2CH_2CH_2CH_2Si$), 29.0 ($SiCH_2CH_2S$), 34.2 (CH_2COOH), not observed ($SCH_2CH_2CH_2CH_2Si$), 174.3 ($COOH$); **{^{1}H-^{29}Si}**: δ 1.8 (3 $SiCH_3$), 2.7 (4 $SiCH_3$). **MS:** $[M + Na]^+$: 1619.0, $[M - H + Na + NH_4]^+$: 1636.00, $[M - 2 H + Na + 2 NH_4]^+$: 1653.00, $[M - 3 H + Na + 3 NH_4]^+$: 1670.00, $[M - 4 H + Na + 4 NH_4]^+$: 1687.00. **Elemental Analysis:** Calcd.: C, 45.88; H, 7.70; S, 18.07; Obt.: C, 44.96; H, 7.67; S, 18.01.

$HSG_1(S\text{-}CO_2Na)_2$ (**7**). To a THF/H_2O solution (ca. 10 mL) of compound **4** (1.45 g, 3.90 mmol) $NaHCO_3$ (0.69 g, 8.19 mmol) was added and the mixture was stirred at 25ºC for 12 hours. Afterwards, volatiles were removed under vacuum and the residue was dissolved in water and purified by nanofiltration affording compound **7** as a yellow solid (1.29 g, 80 %). Data for **7**: $C_{13}H_{24}Na_2O_4S_3Si$ (414.59 g.mol^{-1}). **NMR (D_2O): ^{1}H**: δ 0.00 (s, 3 H, $SiCH_3$), 0.54 (m, 2 H, $SCH_2CH_2CH_2CH_2Si$), 0.86 (m, 4 H, $SiCH_2CH_2S$), 1.37 (m, 2 H, $SCH_2CH_2CH_2CH_2Si$), 1.66 (m, 2 H, $SCH_2CH_2CH_2CH_2Si$), 2.57 ($SiCH_2CH_2S$), 2.65 (m, 2 H, $SCH_2CH_2CH_2CH_2Si$), 3.17 (s, 4 H, SCH_2CO_2); **^{13}C{^{1}H}**: δ -5.4 ($SiCH_3$), 13.1 ($SCH_2CH_2CH_2CH_2Si$), 13.9 ($SiCH_2CH_2S$), 24.0 ($SCH_2CH_2CH_2CH_2Si$, $SCH_2CH_2CH_2CH_2Si$), 27.8 ($SiCH_2CH_2S$), 36.9 (SCH_2CO_2), 38.5 ($SCH_2CH_2CH_2CH_2Si$), 178.0 (CO_2Na); **{^{1}H-^{29}Si}**: δ 2.8 ($SiCH_3$). **MS:** $[M+ Na^+ + H^+]^+$: 415.0; $[MNa_2 + Na^+]^+$: 437.0. **Elemental Analysis:** Calcd.: C, 37.66; H, 5.83; S, 23.20; Obt.: C, 38.01; H, 5.90; S, 23.50.

$HSG_2(S\text{-}CO_2Na)_4$ (**8**). Following the procedure described for compound **7**, compound **8** was obtained (0.52 g, 90 %) as a yellow solid from the reaction of **5** (0.56 g, 0.71 mmol) with $NaHCO_3$ (0.36 g, 4.28 mmol). Data for **8**: $C_{29}H_{54}Na_4O_8S_5Si_3$ (867.27 g.mol^{-1}). **NMR (D_2O): ^{1}H**: δ -0.08 (s, 3 H, $SiCH_3$), -0.02 (s, 6 H, $SiCH_3$), 0.48 (m, 2 H, $SCH_2CH_2CH_2CH_2Si$), 0.57 (m, 8 H, $SiCH_2CH_2CH_2Si$), 0.86 (m, 8 H, $SiCH_2CH_2S$), 1.33 (m, 6 H, $SCH_2CH_2CH_2CH_2Si$, $SiCH_2CH_2CH_2Si$), 1.65 (m, 2 H, $SCH_2CH_2CH_2CH_2Si$), 2.57 ($SiCH_2CH_2S$), 2.65 (m, 2 H, $SCH_2CH_2CH_2CH_2Si$), 3.13 (s, 8 H, SCH_2CO_2); **^{13}C{^{1}H}**: δ -5.5 (1 $SiCH_3$), -4.8 (2 $SiCH_3$), 13.6 ($SCH_2CH_2CH_2CH_2Si$), 13.9 ($SiCH_2CH_2S$), 18.2, 18.4, ($SiCH_2CH_2CH_2Si$), 24.1 ($SCH_2CH_2CH_2CH_2Si$, $SCH_2CH_2CH_2CH_2Si$), 27.8 ($SiCH_2CH_2S$), 36.9 (SCH_2CO_2), 38.8 ($SCH_2CH_2CH_2CH_2Si$), 178.0 (CO_2Na); **{^{1}H-^{29}Si}**: δ 1.8 (1 $SiCH_3$), 2.2 (2 $SiCH_3$). **Elemental Analysis:** Calcd.: C, 40.16; H, 6.28; S, 18.49; Obt.: C, 44.14; H, 7.50; S, 17.80.

$HSG_3(S\text{-}CO_2Na)_8$ (**9**). Following the procedure described for compound **7**, compound **9** was obtained (0.52 g, 90 %) as a yellow solid from the reaction of **6** (0.69 g, 0.43 mmol) with $NaHCO_3$ (0.36 g, 4.31 mmol). Data for **9**: $C_{61}H_{114}Na_8O_{16}S_9Si_7$ (1772.65 g.mol^{-1}). **NMR (CD_3OD): ^{1}H**: δ -0.07 (s, 6 H, $SiCH_3$), 0.00 (s, 12 H, $SiCH_3$), 0.57 (m, 18 H, $SiCH_2CH_2CH_2Si$, $SCH_2CH_2CH_2CH_2Si$), 0.87 (m, 16 H, $SiCH_2CH_2S$), 1.32 (m, 14 H, $SCH_2CH_2CH_2CH_2Si$, $SiCH_2CH_2CH_2Si$), 1.61 (m, 2 H, $SCH_2CH_2CH_2CH_2Si$), 2.56 (m, 18 H, $SCH_2CH_2CH_2CH_2Si$, $SiCH_2CH_2S$), 3.16 (s, 16 H, SCH_2CO_2); **^{13}C{^{1}H}**: δ -5.2 (3 $SiCH_3$), -4.4 (4 $SiCH_3$), not observed ($SCH_2CH_2CH_2CH_2Si$), 13.8 ($SiCH_2CH_2S$), 18.4, 18.6 ($SiCH_2CH_2CH_2Si$), not observed ($SCH_2CH_2CH_2CH_2Si$), not observed ($SCH_2CH_2CH_2CH_2Si$), 27.8 ($SiCH_2CH_2S$), 36.9 (SCH_2CO_2), not observed ($SCH_2CH_2CH_2CH_2Si$), 178.0 (CO_2Na); **{^{1}H-^{29}Si}**: δ 1.1 (3 $SiCH_3$), 2.1 (4 $SiCH_3$). **MS:** $[M + Na]^+$: 1619.41.

Elemental Analysis: Calcd.: C, 41.33; H, 6.48; S, 16.28; Obt.: C, 41.81; H, 6.78; S, 16.49.

2.3.2. Dendronized gold-nanoparticle (GNP) synthesis

GNPs coated with sulfonate (STC-GNP) terminated and trimethylammonium (ATC-GNP) terminated carbosilane dendrons were synthetized according to the method described by Peña-González et al. [21, 22]. Figure 1 shows a schematic drawing of GNPs coated with sulfonate (STC-GNP) and trimethylammonium (ATC-GNP) carbosilane dendrons from first to third generation (1G-3G). The size of whole GNPs was smaller than 5 nm.

$AuG_1(S\text{-}(CO_2Na)_2)$ (10). To an aqueous solution of $HAuCl_4$ (30 mL, 0.90 mmol, 30 mM) was added dropwise an aqueous solution of compound **7** (80 mL, 0.50 mmol, 6.25 mM). Afterward, $NaBH_4$ in water (25 mL, 5.00 mmol, 200 mM) was added dropwise, and the mixture was stirred another 4 h. Nanoparticles were purified by dialysis (MWCO 10,000) affording **10** (200 mg, stored in deionized water at 4 ºC). Data for **10**: $Au_{1090}(C_{13}H_{23}Na_2O_4S_3Si)_{206}$. (Av.Mw.299885.94 $gmol^{-1}$). **^{1}H NMR (D_2O):** δ 0.09 (s, $SiCH_3$), 0.52 (m, $SCH_2CH_2CH_2CH_2Si$), 0.81 (m, $SiCH_2CH_2S$), 1.17 (m, $SCH_2CH_2CH_2CH_2Si$), 2.53 ($SiCH_2CH_2S$), 3.09 (s, 4 H, SCH_2CO_2). **Au/L reactant molar ratio** = 2:1. **TGA (%):** Au, 71.57; (L), 28.43. **Calc. molar ratio Au/L** = 5.29:1 in the nanoparticles. **UV-Vis (SPR):** 521.3 nm. **Zeta potential (mV):** -33.0. **Mean diameter of gold core (TEM):** D = 3.3 nm. N_{Au} = 1090; N_L = 206.

$AuG_2(S\text{-}(CO_2Na)_4)$ (11). Following the procedure described for compound **10**, compound **11** was obtained (220 mg) from the reaction of $HAuCl_4$ (30 mL, 0.90 mmol, 30 mM) with compound **8** (80 mL, 0.25 mmol, 3.12 mM) and $NaBH_4$ (25 mL, 5.00 mmol, 200 mM) Nanoparticles were purified by dialysis (MWCO 10,000) Data for **11**: $Au_{3416}(C_{29}H_{53}Na_4O_8S_5Si_3)_{648}$ (Av.Mw.1234158.32 $gmol^{-1}$). **^{1}H NMR (D_2O):** -0.02 (s, 1 $SiCH_3$), -0.00 (s, 2 $SiCH_3$), 0.46 (m, $SCH_2CH_2CH_2CH_2Si$), 0.55 (m, $SiCH_2CH_2CH_2Si$), 0.84 (m, $SiCH_2CH_2S$), 1.20 (m, $SCH_2CH_2CH_2CH_2Si$, $SiCH_2CH_2CH_2Si$), 2.52 (m, $SiCH_2CH_2S$), 3.10 (s, SCH_2CO_2). **Au/L reactant molar ratio** = 4:1. **TGA (%):** Au, 54.41; (L), 4559. **Calc. molar ratio Au/L** = 5.25:1 in the nanoparticles. **UV-Vis (SPR):** 528.3 nm. **Zeta potential (mV):** -31.0. **Mean diameter of gold core (TEM):** D = 4.8 nm. N_{Au} = 3416; N_L = 648.

$AuG_3(S\text{-}(CO_2Na)_8)$ (12). Following the procedure described for compound **10**, compound **12** was obtained (520 mg) from the reaction of $HAuCl_4$ (30 mL, 0.90 mmol, 30 mM) with compound **9** (80 mL, 0.13 mmol, 1.58 mM) and $NaBH_4$ (25 mL, 5.00 mmol, 200 mM) Nanoparticles were purified by dialysis (MWCO 10,000) Data for **12**: $Au_{3702}(C_{61}H_{113}Na_8O_{16}S_9Si_7)_{356}$ (Av.Mw.1359853.32 $gmol^{-1}$). **^{1}H NMR (D_2O):** -0.05 (s, 3 $SiCH_3$), 0.02 (s, 4 $SiCH_3$), 0.55 (m, $SiCH_2CH_2CH_2Si$, $SCH_2CH_2CH_2CH_2Si$), 0.85 (m,

SiCH_2CH$_2$S), 1.22 (m, SCH$_2$CH$_2$CH_2CH$_2$Si, SiCH$_2$CH_2CH$_2$Si), 2.54 (m, SiCH$_2$CH_2S), 3.14 (s, SCH_2CO$_2$). **Au/L reactant molar ratio** = 8:1. **TGA (%):** Au, 53.65; (L), 46.35. **Calc. molar ratio Au/L** = 10.41:1 in the nanoparticles. **UV-Vis (SPR):** 527.9 nm. **Zeta potential (mV):** -42.0. **Mean diameter of gold core (TEM):** D = 4.9 nm. $\boldsymbol{N_{Au}}$ = 3702; $\boldsymbol{N_L}$ = 356.

2.3.3. Fluorescence measurements

Fluorescence of standard proteins (BSA, Lyz, and Myo) in presence or absence of GNPs was measured on a RF-1501 spectrofluorometer (Shimadzu, Kyoto, Japan). The excitation wavelength was set at 280 nm and the fluorescence emission spectra was recorded in the range from 290 to 400 nm. Concentrations of BSA, Lyz, and Myo were set at 0.2 μM while different dendronized GNPs concentrations (0.005-0.2 μM) were added. Solutions were prepared at acid (0.1 % TFA), neutral (water), and basic (5 mM Tris-HCl, pH 10.0) pHs for STC-GNP and ATC-GNPs, and at acid and basic pHs for CTC-GNP.

2.4. Protein extraction from a complex vegetable matrix

Extraction of proteins from defatted peach seeds was carried out using two methods. Method 1 was a conventional extraction (CE) procedure reported by Vásquez-Villanueva et al. [23]. Briefly, a buffered solution containing 100 mM Tris-HCl (pH 7.5) and 0.5 % (w/v) of SDS and DTT was added to the peach seeds. The blend was sonicated using a high intensity focused ultrasound (HIFU) probe (model VCX130, Sonic Vibra-cell, Hartford, CT, USA) for 1 min at 30 % of amplitude. After centrifugation for 10 min, supernatant containing proteins was precipitated with cold acetone for 15 min. Method 2 involved the direct addition of GNPs to the defatted seeds followed by shaking for, at least, 2 h. Supernatant containing proteins interacting with GNPs was filtered for 90 min at 4000xg through 100 kDa molecular weight cut-off (MWCO) filters Amicon Ultra-4 (Merck Millipore, Tullagreen, Ireland). Protein-GNP interactions were disrupted using 0.1 % SDS and 1M NaCl at room temperature (25 °C)

and at 50 °C, by gently shaking during 45 min. A second ultrafiltration was carried out in order to separate proteins from GNPs after interaction disruption. Proteins released were monitored by Bradford assay [24]. Data were expressed as the mean ± standard deviation corresponding to two independent samples measured by triplicate.

2.5. Protein separation by SDS-PAGE

Sodium dodecyl sulfate polyacrylamide gel electrophoresis (SDS-PAGE) was carried out using a Bio-Rad Mini-protean system (Hercules, CA, USA). Protein solutions, at a 1:1 v/v ratio, were prepared in Laemmli buffer that contained 5 % (v/v) β-mercaptoethanol. The mixture was boiled at 100 °C for 5 min and loaded into the precast gel. A solution containing standard proteins with MWs from 10 to 250 kDa was loaded into the first well. Tris/glycine/SDS was used as running buffer. Separation conditions were: 80 V for 5 min and from 80 to 150 V in 40 min. After protein separation, the gel was dipped in a solution containing water/MeOH/AA (50/40/10 % (v/v)) with shaking during 30 min for fixing proteins. Afterwards, a second fixing solution containing EtOH/AA (10/5 % v/v) was added, followed by shaking for 15 min. This step was carried out twice. Next, a 10 % of oxidizer solution was added to the gel and washed several times with Milli-Q water until yellow color is completely removed from the gel. Gel staining for low protein concentration samples was carried out with a silver reagent by shaking during 20 min following by washing for 1 min and addition of a developer. The reaction was stopped with 5 % AA. For high protein concentration samples, after first fixing solution, gels were stained with Coomassie Blue for 1 h, followed by washing until removal of the deep blue color.

Transmission electron microscopy (TEM). TEM were performed using a ZEISS EM10 TEM with 30 µm lens and a side-mounted 1K CCD Camera, operating at an acceleration voltage of 100 kV and with 0.2 nm resolution. The samples were prepared

by dropping a dilute solution containing the nanoparticles on a carbon-coated copper grid (400 mesh) and dried before observation and measurement (particles size measurements were performed using Image J).

Zeta Potential and Dynamic Light Scattering (DLS).

The zeta-potential of compounds were measured using a Zetasizer Nano ZS (Malvern Instruments Ltd., UK) at 25 ºC in a disposable Malvern plastic cuvette. The solutions were prepared by solving 1 mg of each compound in 1 mL of purified water, which was previously filtered through 0.22 µm syringe filter.

Thermogravimetric Analysis (TGA). The thermogravimetrics analyses were performed using a Q500 from TGA instruments. Dry and pure samples (2 - 10 mg) were placed into platinum sample holder under nitrogen atmosphere. The measurements were recorded from 25 to 1000 ºC, with heating rate of 10 ºC/min.

UV-vis optical Spectroscopy. The UV-visible absorption measurements were performed using a Perkin-Elmer Lambda 18 spectrophotometer. The spectra were recorded by measuring dilute samples in a quartz cell with a path length of 1 cm.

3. Results and discussion

Previous studies demonstrated the interaction of proteins with carbosilane dendrimers (sulfonate and carboxylate) and dendron coated single wall carbon nanotubes obtaining very interesting results that, in some cases, resulted in applications in protein sample preparations [14-16]. On the other hand, sulfonate- (STC) and trimethylammonium- (ATC) terminated carbosilane dendron coated GNPs have previously been synthesized and could also be of interest in protein sample preparation. ATC-GNPs are positively

charged at all pHs due to their NMe_3^+ groups and show MWs of 64, 201, and 307 kDa [22] while SCT-GNPs are negatively charged and show MWs of 597, 378 and 200 kDa (see Figure 1) [21]. Both present particle sizes around 5 nm. Although they have never been applied in protein sample preparation, their characteristics make them very attractive for this purpose. Additionally, taking into account the performance of carboxylate carbosilane dendrimers for the extraction of proteins, the synthesis and application of carboxylate-terminated dendron coated GNPs is of great interest.

3.1. Synthesis and characterization of carboxylate terminated dendron coated GNPs

3.1.1. Synthesis of dendrons

As commented above, GNPs can be stabilized employing dendrons containing the functions of interest on the surface and a thiol moiety at the focal point for grafting to gold surface. Hence, the first step is to find an adequate procedure to develop new dendrons with peripheral carboxylate groups and thise thiol function. For better understanding of the work, the dendrons are named as $XG_n(Y)_m$, where X indicates the nature of the focal point, G_n the dendron generation and $(Y)_m$ the peripheral function and its number (V for vinyl, Scheme 1).

As we have published, thiol-ene addition is a versatile protocol for carbosilane dendron modification [E. Fuentes-Paniagua, C. E. Peña-González, Marta Galán, R. Gómez, F. J. de la Mata, J. Sánchez-Nieves, Thiol-Ene Synthesis of Cationic Carbosilane Dendrons: a New Family of Synthons. *Organometallics* **2013**, *32*, 1789−1796]. Thus, starting from vinyl terminated dendrons and a protected thiol at the focal point, $MeCOSG_nV_m$ (n = 1, m = 2; n =2, m = 4; n = 3, m =8), the reaction with the thiol-ester derivative $HSCH_2CO_2Me$ afforded the dendrons with ester groups $MeCOSG_n(CO_2Me)_m$ (n = 1, m = 2 (**1**); n =2, m = 4 (**2**); n = 3, m =8 (**3**)) (Scheme 1), precursor of carboxylate

functions, at the periphery. These compounds were obtained as orange oils with moderate yields. ^{1}H-NMR spectroscopy (Figure S1) showed the disappearance of the vinyl functions (around 6 ppm) and formation of the chain $Si(CH_2)_2S$ from the thiol-ene addition (around 0.9 ppm for $SiCH_2$ and 2.6 ppm for CH_2S). The presence of the terminal groups was also observed in the ^{1}H-NMR spectra (around 3.2 for SCH_2CO and around 3.7 ppm for MeCO). In a similar way, ^{13}C-NMR spectroscopy also confirmed formation of dendrons **1-3** (Figure S1), standing out the resonance for the carbon atom of the ester group at about 196 ppm.

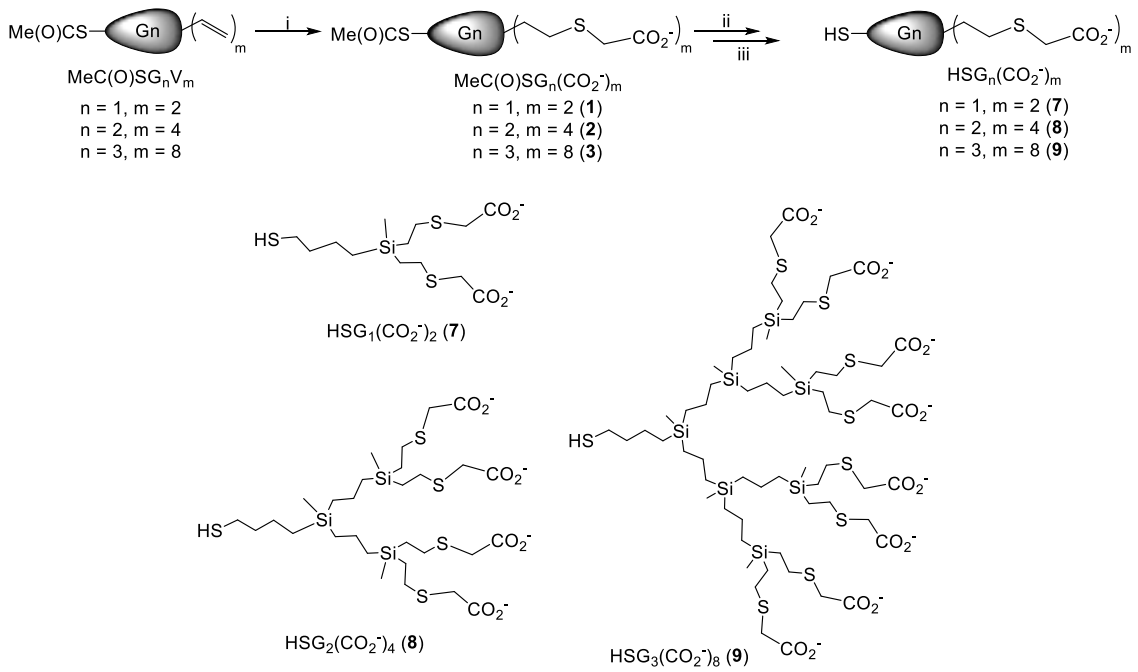

Scheme 1. Synthesis and structures of carboxylate dendrons $HSG_n(CO_2^-)_m$ (n = 1, m = 2 (**7**); n = 2, m = 4 (**8**); n = 3, m = 8 (**9**)) (anions omitted for clarity). i) $HSCH_2CO_2^-$, DMPA, hν; ii) NaOH, HCl; iii) $HNaCO_3$.

Next step was deprotection of both peripheral and focal point moieties. This process was achieved by addition of excess NaOH and subsequent neutralization with HCl. This is necessary because under strong basic conditions the focal point would be present probably as thiolate. With this procedure, the corresponding neutral dendrons $HSG_n(CO_2H)_m$ (n = 1, m = 2 (**4**); n =2, m = 4 (**5**); n = 3, m =8 (**6**)) were obtained as

light orange oils in high yield. The more noticeable changes in NMR spectroscopy were the disappearance of both methyl groups bound to the carbonyl carbon atoms. On the other hand, the HS resonance was observed about 1.4 ppm, in the ^{1}H-NMR spectra, and the new carbonyl around 174.5, in the ^{13}C-NMR spectra (Figure S2).

Finally, the goal carboxylate dendrons $HSG_n(CO_2^-)_m$ (n = 1, m = 2 (**7**); n =2, m = 4 (**8**); n = 3, m =8 (**9**)) were obtained by addition of excess $HNaCO_3$. This new compounds were obtained in high yield as pale yellow solids soluble in water. NMR spectroscopy confirmed that after reaction the dendron structure was maintained (Figures S3), observing in the ^{13}C-NMR spectra the resonance corresponding to the carboxylate carbon atom around 178 ppm.

3.1.2. Synthesis of GNPs

The CTC-GNPs were prepared using the Brust-Schiffrin method (or direct method) by reaction of the gold precursor [$AuCl_4^-$] with the dendrons $HSG_n(CO_2^-)_m$ (**7-9**) in the presence of a reducing agent ([BH_4^-]) and using water as solvent. The ratio Au/dendron used for this reaction was m/1, being m the number of peripheral carboxylate groups. This ratio was chosen taking into account previous results from the synthesis of related sulfonated SCT-GNP, which showed the ability of anionic groups to interact with gold cations avoiding NP growing [21] Peña-González C. E., García-Broncano P., Ottaviani M. F., Cangiotti M., Fattori A., Hierro-Oliva M., González-Martín M. L., Pérez-Serrano J., Gómez R., Muñoz-Fernández M. A., Sánchez-Nieves J., de la Mata F. J. Dendrionized anionic gold nanoparticles: Synthesis. Characterization, and antiviral activity. Chemistry European Journal 22 (2016) 2987-2999. After purification, CTC-GNPs ($AuG_n(S\text{-}(CO_2^-)_m)$; n = 1, m = 2 (**10**); n =2, m = 4 (**11**); n = 3, m =8 (**12**)) were obtained and kept in water suspension to avoid aggregation. However, unfortunately

only 1G was soluble in this solvent. The GNPs were characterized (Table X) by NMR, TGA, UV, TEM, potential Z and DLS.

CTC-GNPs showed MWs of 300, 1234, and 1359 kDa for 1G, 2G, and 3G, respectively. The sizes of these GNPs (TEM, Figure X) were slightly bigger than the corresponding sulfonate STC-NPs, but for 1G CTC-GNP which showed a similar value (see Figure 1). Regarding the hydrodynamic size, measured by DLS, the value obtained was of 28.2 nm. This difference can be attributed to interactions between NPs in solution. This diameter value obtained by DLS and the corresponding polydispersity (PDI) can be used to calculate a theoretical diamenter (Cdn = 4.71 nm, Table X), which approximates to that observed by TEM) [Hanus, L.H., Ploehn, H.J., 1999. Conversion of intensity-averaged photon correlation spectroscopy measurements to number-Averaged particle size distributions. 1. Theoretical development. Langmuir 15, 3091]. The potential Z of 1G CTC-GNP was negative (-32.4 V) as expected. For the other two CTC-GNP, 2G and 3G, this measure could not be done due to the precipitation of the samples. In UV spectra were observed the band corresponding to the plasmon resonance around 525 nm. The ^{1}H-NMR spectra showed the resonances corresponding to the dendron.

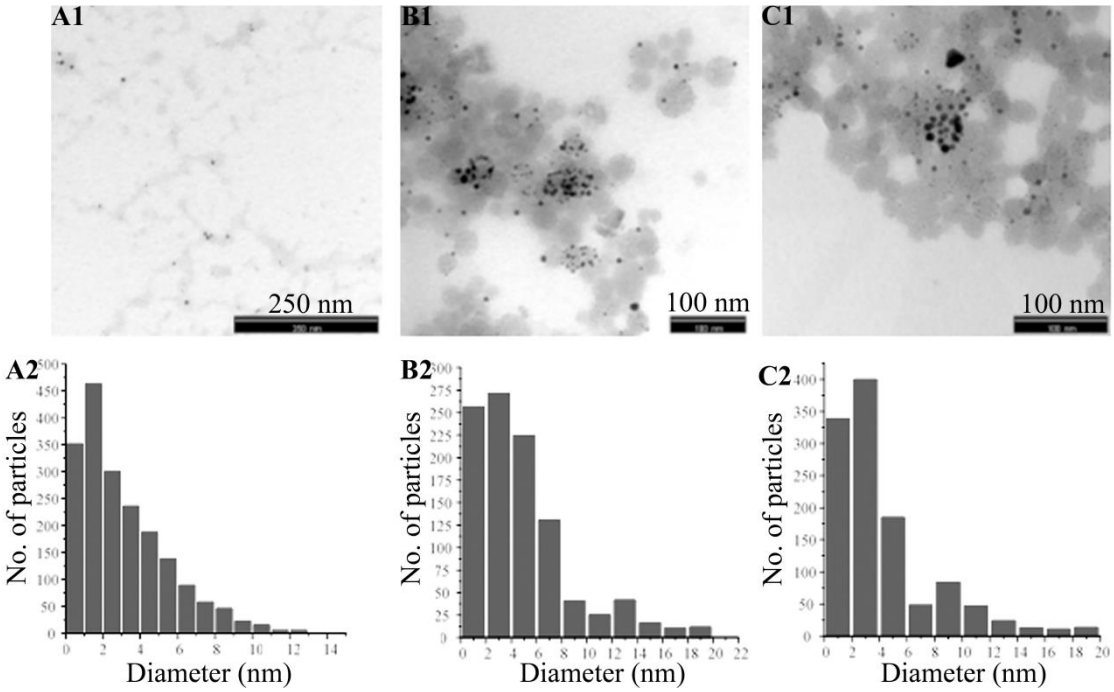

Figure X. TEM images and distribution histograms of CTC-GNPs **10** (A), **11** (B) and **12** (C).

CTC-GNPs	Molar Ratio M/L[a]		d_n[b]	d_z[c]	Cd_n[d]	PDI[e]	MF[f]	MW[f]	N[g]	ZP[h]	UV-Vis[i]
	Theoretic	Obtained									
$AuG_1(S\text{-}(CO_2Na)_2)$ (**10**)	2:1	5.3:1	3.3	28.2	4.71	0.43	$Au_{1090}(C_{13}H_{23}Na_2O_4S_3Si)_{206}$	299885.94	412	-32.4	521.3
$AuG_2(S\text{-}(CO_2Na)_4)$ (**11**)	4:1	5.3:1	4.8	-	-	-	$Au_{3416}(C_{29}H_{53}Na_4O_8S_5Si_3)_{648}$	1234158.32	2592	-	525.8
$AuG_3(S\text{-}(CO_2Na)_8)$ (**12**)	8:1	10.4:1	4.9	-	-	-	$Au_{3702}(C_{61}H_{113}Na_8O_{16}S_9Si_7)_{356}$	1359853.32	2848	-	526.2

Table X. Selected data of dendronized AuNPs with dendrons **7-9**. a) L refers to dendron; b) Diameter (d_n, nm) obtained by TEM, corresponds with the mode value; c) Diameter (d_z, nm) obtained by DLS; d) d_n (nm) calculated ($Cd_n = d_z/(1+Q)^5$; Q corresponds with PDI) [Hanus, L.H., Ploehn, H.J., 1999. Conversion of intensity-averaged photon correlation spectroscopy measurements to number-Averaged particle size distributions. 1. Theoretical development. Langmuir 15, 3091]; e) Polydispersity index (PDI) obtained by DLS; f) Molecular formula (MF) and weight (MW, $gmol^{-1}$) obtained from TEM and TGA (see Experimental Section); g) Number of $-SO_3^-$ groups by NP; h) Zeta potential (mV); i) Ultraviolet-Visible band absorption (nm).

3.2. Study of interactions between proteins and dendron coated GNP

Protein-GNP interactions were evaluated by monitoring the intrinsic fluorescence intensity of proteins (mainly due to tryptophan (Trp) residues) and the maximum emission wavelength. The monitorization of the intrinsic fluorescence of proteins is frequently used to study changes in the local protein environment such as protein folding/unfolding and protein interactions. In fact, these protein structure changes can modify Trp residues exposure resulting in variations in proteins fluorescence intensity and maximum emission wavelengths [25, 27].

Three different standard proteins (BSA, Lyz, and Myo) were used in these studies. Their MWs, isoelectric points (pI), charge at different pHs, and number of Trp residues are summarized in Table 1.

3.2.1. Interactions between sulfonate-terminated carbosilane dendron-coated GNPs and proteins

Figure 2 shows the fluorescence intensity when increasing concentrations of STC-GNP (1G, 2G, 3G) were added to protein standard solutions (BSA, Lyz, and Myo) at different pHs (pH 2.5, 6.5, and 10.0). Fluorescence intensity decreased at all pHs and with all generations with the STC-GNP concentration, although this behavior was more significant at acid and neutral pH. Fluorescence decrease was more pronounced for Lyz, especially at neutral and basic pHs. Indeed, while BSA and Myo are only positively charged at acid pH, Lyz is positively charged at all tested pHs, which favors the establishment of electrostatic interactions with STC-GNPs. Moreover, Lyz is the protein with the highest number of Trp residues and the smallest size, which also favors its access to sulfonate groups. Similar behavior was observed in the case of sulfonate-terminated carbosilane dendron-coated nanotubes [16].

Unlike Lyz, BSA and Myo did not show net positive charge at neutral and basic pHs, although both proteins show a decreasing fluorescence intensity with GNP concentration. Nevertheless, even when the overall charge in proteins is negative or null, they contain local positively charged sites where electrostatic interactions with GNPs could occur and, thus, justify fluorescence deactivation. Moreover, additional molecular interactions such as hydrophobic interactions and van der Waals forces could also be possible [29]. Concerning to dendron generation, STC-GNP capped with first generation dendrons generally showed the highest decreases in fluorescence intensity. This could be justified by the higher number of functional groups (see Figure 1) that contains 1G STC-GNP. Moreover, in most cases, fluorescence decrease came along with blue shifts in maximum emission wavelengths.

In order to confirm that the decrease in the intrinsic fluorescence intensity of proteins was due to interactions with GNPs and not to fluorescence deactivation by dynamic quenching, solutions were filtered through 100 kDa cut-off filters so that formed complexes, if any, could be separated from the remaining solution. Proteins in complexes were next separated and detected by SDS-PAGE. Figure 3 shows how the intensity of the band corresponding to BSA increased when increasing the GNP concentration, which confirmed the formation of complexes between BSA and GNPs. No band would be expected if dynamic deactivation of fluorescence had occurred.

3.2.2. Interactions between carboxylate-terminated carbosilane dendron-coated GNP and proteins

CTC-GNPs present different behavior depending on the pH. At acid pH, they are protonated and precipitated while at basic pHs, they are negatively charged and in solution. Figure 4 shows the protein fluorescence variation when adding CTC-GNP at acid and basic pHs. In general, fluorescence intensity decreased with the dendron

concentration at both pHs and for all generations. Fluorescence decrease at acid pH came along, in some cases, with the formation of a precipitate. This behavior reminded to previous results in which carboxylate terminated dendrimers formed insoluble complexes with proteins [15]. Nevertheless, in this case the precipitate only appeared for the smallest proteins, Lyz and Myo, with the smallest CTC-GNPs (1G and 2G) at the highest GNP concentrations. No precipitate was observed with the biggest CTC-GNP (3G) or with the biggest protein, BSA, at any generation and GNP concentration. At basic pH, the highest decrease in fluorescence intensity was observed for Lyz that showed positive charge while negative BSA and neutral Myo showed less significant variations. In these cases, fluorescence quenching could be explained by interactions through local cationic sites of the proteins or by other forces different to electrostatic. Like previously, fluorescence decrease came along with blue shifts in maximum emission wavelengths in most cases.

3.2.3. Interaction between trimethylammonium-terminated carbosilane dendron-coated GNP and proteins

ATC-GNP are water soluble GNPs that show positive charge at all pHs. No reduction in the fluorescence intensity of proteins was observed at acid pH, which is explained by the fact that both proteins and GNPs are positively charged. Similarly, Lyz neither showed any fluorescence reduction at neutral and basic pHs since it was positively charged at tested pHs. Only BSA could interact with ATC-GNPs at neutral and basic pHs since it was the only protein with negative charge at these pHs and, thus, it was the only that could electrostatically interact with positive ATC-GNPs (see Figure 5).

3.3. Application of STC-GNP, CTC-GNP, and ATC-GNP to protein sample preparation

Previous results demonstrated that the interaction of proteins with GNPs greatly depended on protein nature, pH, and dendrimer generation. Thus, in order to demonstrate the potential of studied nanoparticles in the extraction of proteins from a complex sample, more favoring conditions were selected: 1G, 2G, and 3G STC-GNP at neutral pH, 1G, 2G, and 3 G CTC-GNP at acid pH, and 1G, 2G, and 3G ATC-GNP at basic pH. Selected GNPs and conditions were employed for the extraction of proteins from peach seeds. For that purpose, dispersions of GNPs were mixed with ground peach seeds by shaking. Application of high intensity focused ultrasounds was discarded since it disrupted interactions. Afterwards, GNPs were separated from the remaining solution by ultrafiltration and extracted proteins were separated by SDS-PAGE (see Figure 6). Results were compared with those obtained using a method previously reported [23] that involved a first extraction with a Tris-HCl buffer containing SDS and DTT followed by the purification of proteins by precipitation with acetone. This method was labeled as conventional extraction (CE). Electrophoretic profiles obtained when extraction was carried out with GNPs were similar to the obtained when using the conventional method. Indeed, similar bands below 75 kDa were observed in most cases, while main differences were detected in their intensity. Most intense bands were obtained with STC-GNP and CTC-GNP, highlighting the case of the 2CTC-GNP. In fact, 2G CTC-GNP enabled to extract all the proteins extracted by the conventional method while STC-GNP and 1G and 3G CTC-GNP did not extract some proteins below 20 kDa. As expected, extraction with ATC-GNPs resulted in less intense bands than the observed in the conventional method.

In order to disrupt protein-GNP interactions after protein extraction, different reagents (0.1 % (w/v) SDS and 1M NaCl) and temperatures (room temperature and 50 °C) were applied. Disruption of complexes after their separation is required if we want to work

with extracted proteins and, even, to reutilized GNPs. Released proteins were determined by Bradford assay and results, related to proteins extracted by the conventional method, are grouped in Table 2. Complex disruption at room temperature was less significant than the observed at 50 °C for all GNPs. Moreover, a greater amount of complexes were disrupted with SDS than with NaCl for anionic GNPs while more similar results were observed for the cationic GNPs, for both SDS and NaCl. The highest protein disruption was obtained, as expected, for the 2G CTC-GNP. Released proteins were also separated by SDS-PAGE and electropherograms are shown in Figure 6. As observed, bands intensities, in all cases, were much lower than the observed when proteins were directly separated by SDS-PAGE without previous complex disruption. Although proteins were significantly extracted by interaction with GNPs, disruption conditions seemed to be not strong enough to release proteins interacting with GNPs. In fact, a maximum recovery of 42 % was observed under most favored conditions (2G CTC-GNP). These proteins seem to be those with molecular weights below to 25 kDa while proteins with higher molecular weights were not released from the complexes. Thus, stronger conditions, such as the used in the separation of proteins by SDS-PAGE that contained β-mercaptoethanol, are required to disrupt strong complexes establish between proteins and dendronized GNPs.

4. CONCLUSIONS

This work proposes, for the first time, a route to synthetize carboxylate terminated carbosilane dendronized GNP and demonstrates the potential of different dendronized GNPs (carboxylate terminated, sulfonate terminated, and trimethylammonium terminated) in protein sample preparation. Carboxylate and sulfonate carbosilane dendrons, at acid and neutral pHs, were the most favoring for the interaction of GNPs with proteins. Scarce interactions were observed for positively charged GNPs coated

with trimethylammonium carbosilane dendrons. In most cases, interactions could be electrostatic although forces of other nature could also contribute. Interactions with STC-GNPs were favored with 1G dendrons likely because they have higher number of dendron branches. Interactions with CTC-GNPs were more significant with 2G dendrons probably due to their higher charge density and higher number of dendron branches. CTC-GNPs, at acid pH, formed insoluble complexes with small proteins and the smallest dendrons (1G and 2G) while soluble complexes were observed for bigger proteins and dendrons. Most favoring conditions for the interactions of proteins with STC-, CTC-, and ATC-GNPs were successfully applied for the extraction of proteins in a complex sample. As expected, more suitable dendronized GNPs for the extraction of proteins were STC-GNPs and CTC-GNPs, especially the second generation. A final study to find out the best conditions to break protein-GNP complexes reveled that strength of these interactions that required very harsh conditions for their discruption.

Supporting Information

NMR spectra of dendrons

Aknowledgments

This work was supported by the Spanish Ministry of Economy and Competitiveness (ref. AGL2016-79010-R and CTQ2017-86224-P). R.V.-V thanks the University of Alcalá for the pre-doctoral contract. CIBER-BBN is an initiative funded by the VI National R&D&I Plan 2008-2011, Iniciativa Ingenio 2010, Consolider Program, CIBER Actions and financed by the Instituto de la Salud Carlos III with assistance from the European Regional Development Fund.

REFERENCES

[1] Tiwari P., Vig K., Dennis V., Singh S. Functionalized Gold Nanoparticles and Their Biomedical Applications. Nanomaterials, 1 (2011) 31–63.

[2] Li H., Zhu W., Wan A., Liu, L. The mechanism and application of the protein-stabilized gold nanocluster sensing system. The Analyst. 142 (2017) 567–581.

[3] Brust M., Walker M., Bethell D., Schiffrin D. J., Whyman R. Synthesis of thiol-derivatised gold nanoparticles in a two-phase Liquid–Liquid system. Journal of the Chemical Society, Chemical Communications 0 (1994) 801–802.

[4] Hermes J. P., Sander F., Peterle T., Urbani R., Pfohl T., Thompson D., Mayor M. Gold Nanoparticles Stabilized by Thioether Dendrimers. Chemistry - A European Journal, 17 (2011) 13473–13481.

[5] Elbert K. C., Lee J. D., Wu Y., Murray C. B. Improved Chemical and Colloidal Stability of Gold Nanoparticles through Dendron Capping. Langmuir 34 (2018) 13333-13338.

[6] Newkome G. R., Moorefield C. N., Vögtle F. Dendrimers and Dendrons: Concepts, Synthesis, Applications. Willey-VCH, Weinheim, 2001.

[7] Kalhapure R. S., Kathiravan M. K., Akamanchi K. G., Govender T. Dendrimers-from organic synthesis to pharmaceutical applications: an update. Pharmaceutical Development and Technology 20 (2015) 22-40.

[8] Malik N., Wiwattanapatapee R., Klopsch R., Lorenz K., Frey H., Weener, J., Meijer E.W., W Paulus W., Duncan, R. Dendrimers: Relationship between structure and biocompatibility in vitro, and preliminary studies on the biodistribution of 125I-labelled polyamidoamine dendrimers in vivo. Journal of Controlled Release, 65 (2000) 133–148.

[9] Lee J.H., Cha K.E., Kim M.S., Hong H.W., Chung D.J., Ryu G., Myung H. Nanosized polyamidoamine (PAMAM) dendrimer-induced apoptosis mediated by mitochondrial dysfunction. Toxicology Letters 190 (2009) 202–207.

[10] Labieniec-Watala M., Karolczak K., Siewiera K., Watala C. The Janus Face of PAMAM Dendrimers Used to Potentially Cure Nonenzymatic Modifications of Biomacromolecules in Metabolic Disorders—A Critical Review of the Pros and Cons. Molecules 18 (2013) 13769–13811.

[11] Hatano K., Matsuoka K., Terunuma D. Carbosilane glycodendrimers. Chemical Society Reviews 42 (2013) 4574–4598.

[12] Arnáiz E., Doucede L. I., García-Gallego S., Urbiola K., Gómez R., Tros de Ilarduya C., de la Mata F. J. Synthesis of cationic carbosilane dendrimers via click chemistry and their use as effective carriers for DNA transfection into cancerous cells. Molecular Pharmaceutics 9 (2012) 433-447.

[13] Gras R., Relloso M., García M.I., de la Mata F. J., Gómez R., López-Fernández L. A., Muñoz-Fernández M. A. The inhibition of Th17 immune response in vitro and in vivo by the carbosilane dendrimer 2G-NN16. Biomaterials 33 (2012) 4002-4009.

[14] González-García E., Maly M., de la Mata, F. J., Gómez R., Marina M. L., García M. C. Factors affecting interactions between sulphonate-terminated dendrimers and proteins: A three case study. Colloids and Surfaces B: Biointerfaces 149 (2017) 196-205.

[15] González-García E., Maly M., de la Mata, F. J., Gómez R., Marina M. L., García M. C., Proof of concept of a greener protein purification/enrichment method based on carboxylate-terminated carbosilane dendrimer-protein interactions. Analytical and Bioanalytical Chemistry 408 (2016) 7679-7687.

[16] González-García E., Gutiérrez Ulloa C. E., de la Mata F. J., Marina M. L., García M. C. Sulphonate-terminated carbosilane dendron-coated nanotubes: a greener point of view in protein sample preparation. Analytical and Bioanalytical Chemistry 409 (2017) 5337-5348.

[17] Shcharbin D., Pedziwiatr-Werbicka E., Serchenya T., Cyboran-Mikolajczyk S., Prakhira L., Abashkin V., Dzmitruk V., Ionov M., Loznikova S., Shyrochyna I., Sviridov O., Peña-González C. E., Gumiel A. B., Gómez R., de la Mata F. J., Bryszewska M. Role of cationic carbosilane dendrons and metallic core of functionalized gold nanoparticles in their interaction with human serum albumin. International Journal of Biological Macromolecules 118 (2018) 1773-1780.

[18] Moerz S. T., Huber, P. Protein Adsorption into Mesopores: A Combination of Electrostatic Interaction, Counterion Release, and van der Waals Forces. Langmuir 30 (2014) 2729–2737.

[19] Jin B., Bao W.-J., Wu Z.-Q., Xia X.-H. In Situ Monitoring of Protein Adsorption on a Nanoparticulated Gold Film by Attenuated Total Reflection Surface-Enhanced Infrared Absorption Spectroscopy. Langmuir 28 (2012) 9460– 9465.

[20] Kim Y., Ko S. M., Nam J.-M. Protein-Nanoparticle Interaction-Induced Changes in Protein Structure and Aggregation. Chemistry - An Asian Journal, 11 (2016) 1869–1877.

[21] Peña-González C. E., García-Broncano P., Ottaviani M. F., Cangiotti M., Fattori A., Hierro-Oliva M., González-Martín M. L., Pérez-Serrano J., Gómez R., Muñoz-Fernández M. A., Sánchez-Nieves J., de la Mata F. J. Dendrionized anionic gold nanoparticles: Synthesis. Characterization, and antiviral activity. Chemistry European Journal 22 (2016) 2987-2999.

[22] Peña-González C. E., Pedziwiatr-Werbicka E., Martín-Pérez T., Szewczyk E. M., Copa-Patiño J. L., Soliveri J., Pérez-Serrano J., Gómez R., Bryszewska M., Sánchez-Nieves J., de la Mata F. J. Antibacterial and antifungal properties of dendrionized silver and gold nanoparticles with cationic carbosilane dendrons. International Journal of Phamaceutics 528 (2017) 55-61.

[23] Vásquez-Villanueva R., Marina M. L., García M. C. Revalorization of a peach (*Prunus persica* (L.) Batsch) byproduct: Extraction and characterization of ACE-inhibitory peptides from peach stones. Journal of Functional Foods 18 (2015) 137-146.

[24] Bradford M. M., Rapid and sensitive method for quantitation of microgram quantities of protein utilizing principle of protein-dye binding. Analytical Biochemistry 72 (1976) 248-254.

[25] Eftink M. R. The use of fluorescence methods to monitor unfolding transitions in proteins. Biophysical Journal. 66 (1994) 482-501.

[26] Volden S., Lystvet S. M., Halskau Ø., Glomm W. R. Generally applicable procedure for in situ formation of fluorescence protein gold nanostructures. RSC Advances 2 (2012) 11704-11711.

[27] Lakowicz J. R. Principles of Fluorescence Spectroscopy, Springer, New York, 2006

[28] Joshi D., Soni R. Laser-induced synthesis of silver nanoparticles and their conjugation with protein. Applied Physics A 116 (2014) 635–641.

[29] Treuel L., Malissek M., Grass S., Diendorf J., Mahl D., Meyer-Zaika W., Epple M. Quantifying the influence of polymer coatings on the serum albumin corona formation around silver and gold nanoparticles. Journal of Nanoparticle Research 14 (2012) 1–12.

Figure Captions

Figure 1. Schematic drawing of the first, second, and third generation of the sulfonate-, carboxylate-, and ammonium-terminated carbosilane dendrimer-Gold Nanoparticles (STC-GNP, CTC-GNP, and ATC-GNP, respectively).

Figure 2. Variation of the fluorescence intensity of BSA, Lyz, and Myo with the STC-GNP concentration and generation at different pHs.

Figure 3. Variation of the band intensity of BSA obtained by SDS-PAGE corresponding to the protein that interacted with increasing concentration of 1G STC-GNP at pH 6.5.

Figure 4. Variation of the fluorescence intensity of BSA, Lyz, and Myo with the CTC-GNP concentration and generation at different pHs. ∗ and ☆ indicates the formation of a precipitate.

Figure 5. Variation of the fluorescence intensity of BSA with the ATC-GNP concentration and generation at different pHs.

Figure 6. SDS-PAGE profiles corresponding to the extracted proteins from peach seed using 1G, 2G, and 3G STC-GNP at neutral pH (A left), CTC-GNP at acid pH (B left), and ATC-GNP at basic pH (C left) and corresponding to the released proteins after breakage of protein-GNP complexes with 0.1 % (w/v) SDS and 1 M NaCl (A right, B right, and C right).

Table 1. Mw, isoelectric point (pI), net charge at different pHs, and Trp residues of BSA, Myo, and Lyz at different pHs.

Protein	Mw (kDa)	pI	Charge at Acid pH	Charge at Neutral pH	Charge at Basic pH	Trp residues
BSA	66.5	4.7	+97	-17	-22	Trp 134 Trp 213
Myo	17.8	6.8	+31	0	0	Trp 28 Trp 62 Trp 63 Trp108 Trp111 Trp123
Lyz	14.3	11.35	+20	+9	+7	Trp 7 Trp 14

Table 2. Protein content (%), expressed as mean ± standard deviation, related to the proteins extracted by the conventional method, corresponding to two independent samples measured by triplicate, after disruption of protein-GNP binding with 0.1 (w/v) SDS, and 1 M NaCl at room temperature, and at 50 °C.

	Generation	STC-GNP		CTC-GNP		ATC-GNP	
		25 °C	50 °C	25 °C	50 °C	25 °C	50 °C
SDS	1G	16.3 ± 4.2	40.8 ± 4.3	10.8 ± 4.1	39.9 ± 3.3	5.8 ± 2.1	11.6 ± 2.2
	2G	12.6 ± 1.7	31.7 ± 4.1	11.9 ± 2.9	42.2 ± 2.5	5.2 ± 1.7	10.3 ± 1.0
	3G	11.2 ± 3.2	30.7 ± 2.9	1.6 ± 1.0	9.7 ± 2.9	2.8 ± 1.3	11.3 ± 2.1
NaCl	1G	6.2 ± 4.5	21.6 ± 2.1	3.4 ± 0.9	16.5 ± 2.2	3.4 ± 1.9	25.2 ± 3.4
	2G	5.2 ± 3.4	24.5 ± 1.4	5.8 ± 2.8	28.5 ± 2.4	3.9 ± 1.5	15.3 ± 1.8
	3G	7.1 ± 3.3	28.5 ± 2.3	2.5 ± 1.2	21.2 ± 1.7	5.3 ± 1.2	15.0 ± 2.7

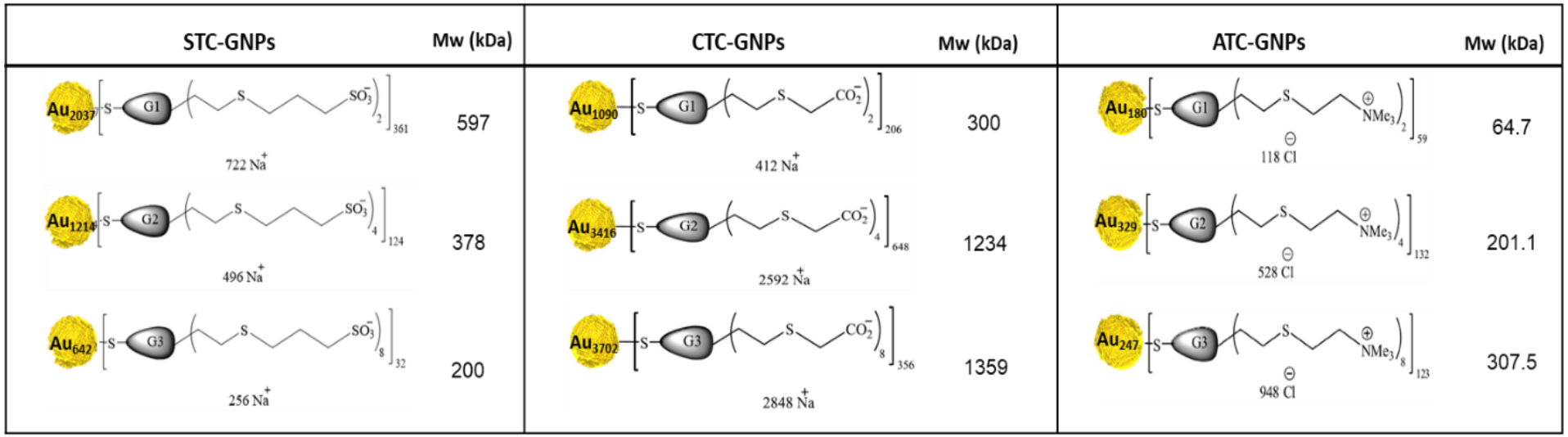
STC-GNPs
Mw (kDa)
CTC-GNPs
Mw (kDa)
ATC-GNPs
Mw (kDa)
Au2037
G1
722 Na+
597
Au1090
G1
412 Na+
300
Au180
G1
118 Cl
64.7
Au1214
G2
496 Na+
378
Au3416
G2
2592 Na+
1234
Au329
G2
528 Cl
201.1
Au642
G3
256 Na+
200
Au3702
G3
2848 Na+
1359
Au247
G3
948 Cl
307.5

Figure 1.

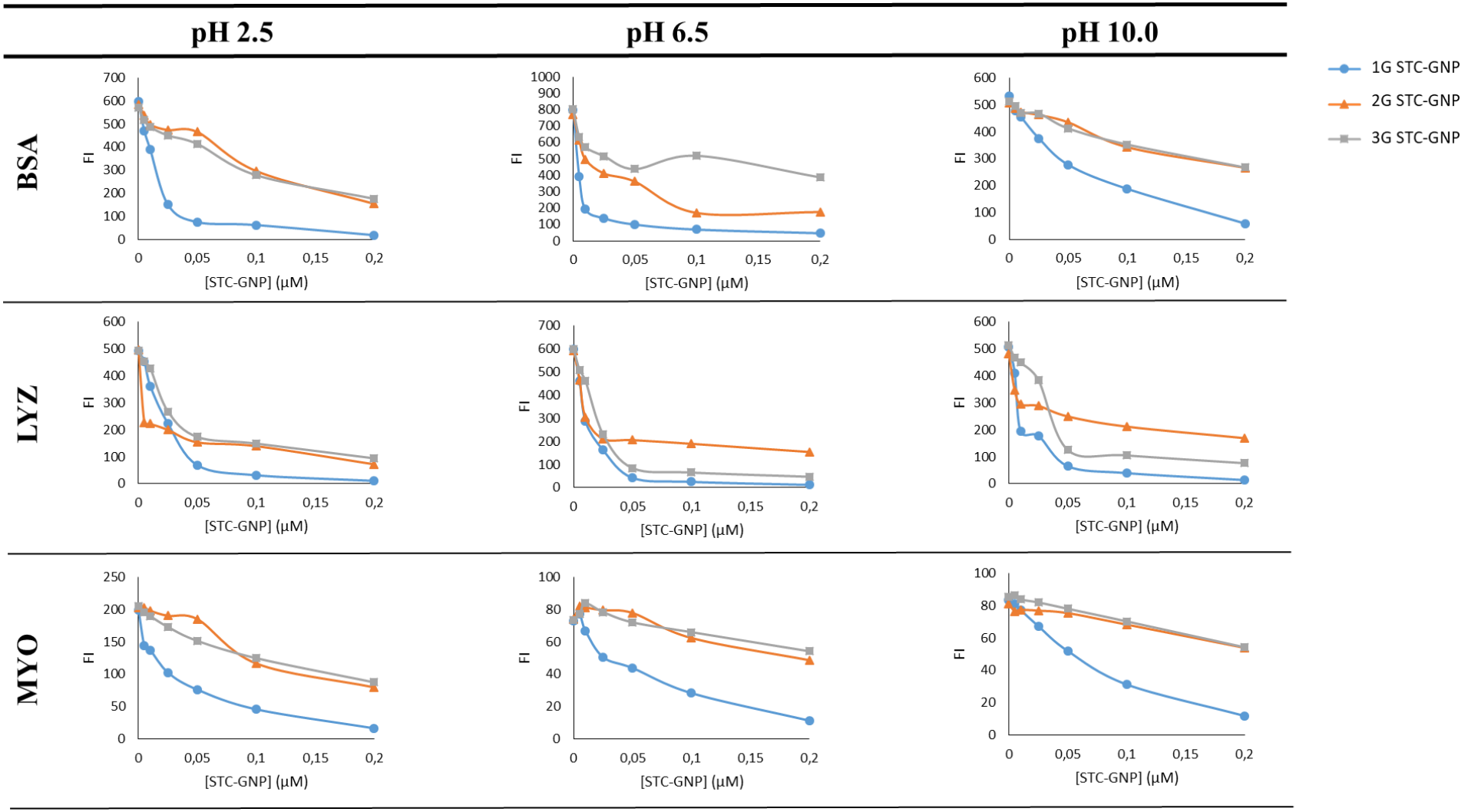
pH 2.5
pH 6.5
pH 10.0
BSA
LYZ
MYO
FI
[STC-GNP] (µM)
1G STC-GNP
2G STC-GNP
3G STC-GNP

Figure 2.

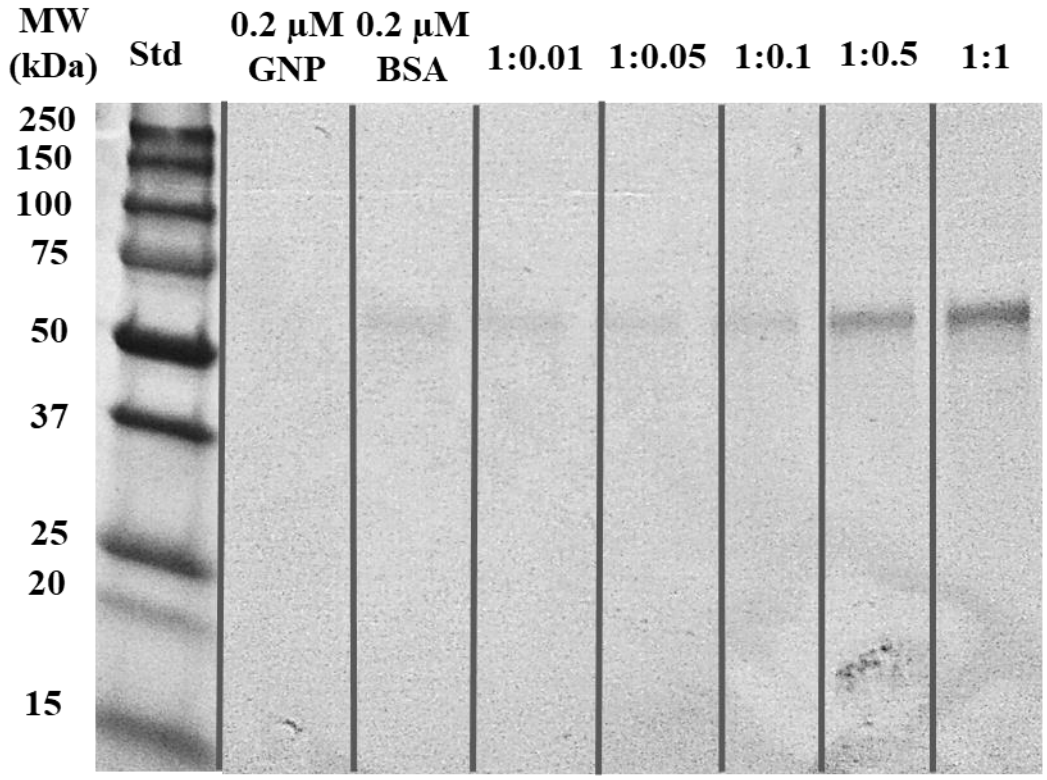
MW
(kDa)
Std
0.2 µM
GNP
0.2 µM
BSA
1:0.01
1:0.05
1:0.1
1:0.5
1:1
250
150
100
75
50
37
25
20
15

Figure 3.

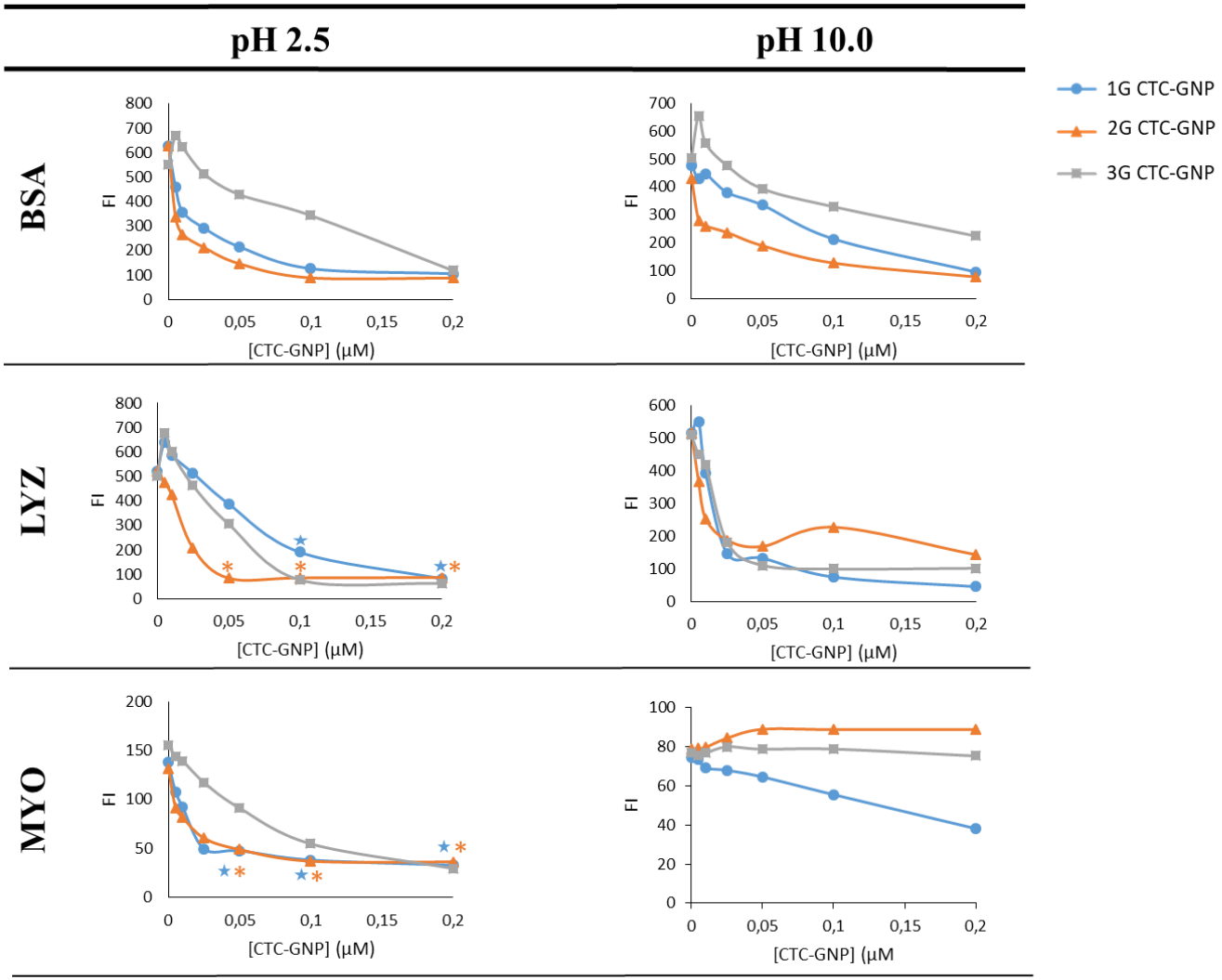
pH 2.5
pH 10.0
BSA
LYZ
MYO
FI
[CTC-GNP] (µM)
1G CTC-GNP
2G CTC-GNP
3G CTC-GNP

Figure 4.

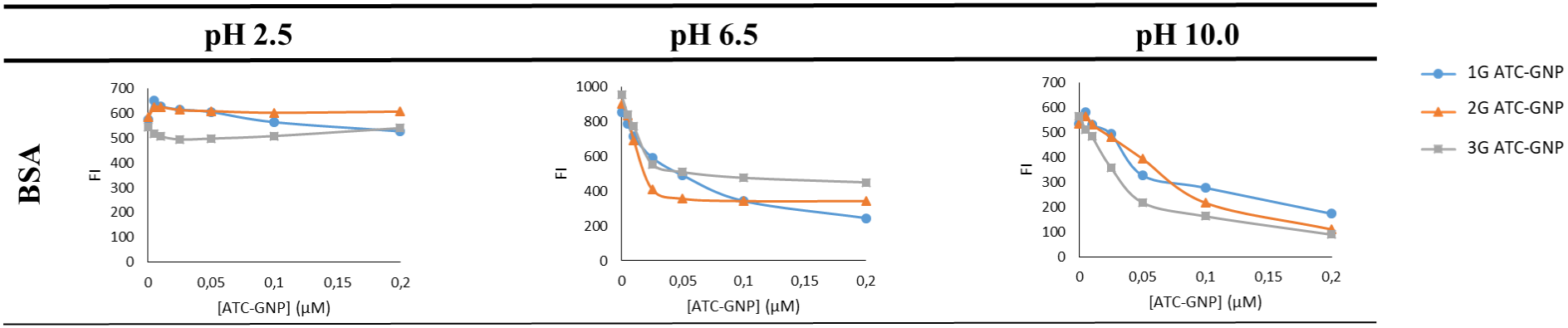
pH 2.5
pH 6.5
pH 10.0
BSA
FI
[ATC-GNP] (µM)
1G ATC-GNP
2G ATC-GNP
3G ATC-GNP

Figure 5.

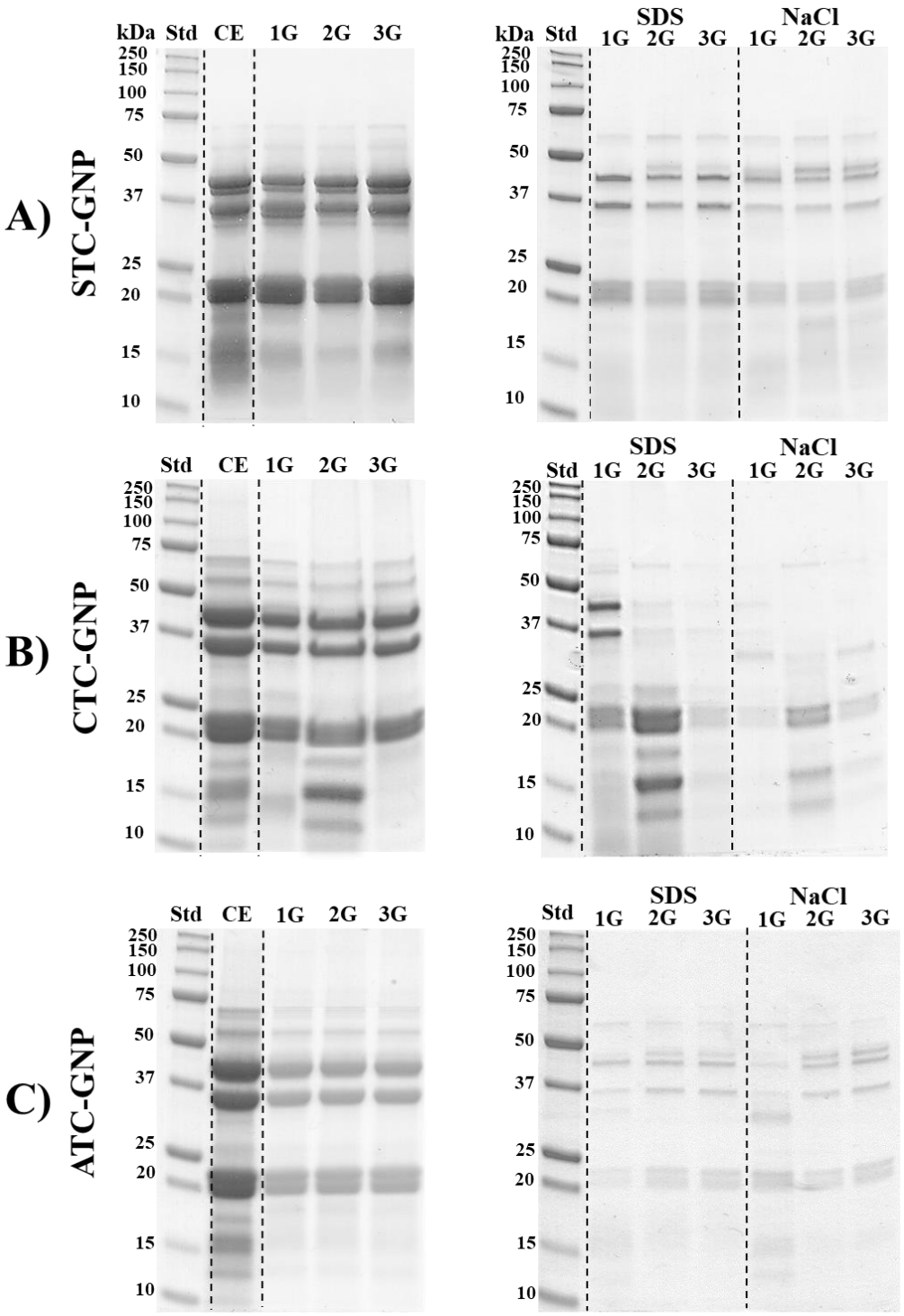
A)
STC-GNP
kDa Std CE 1G 2G 3G
kDa Std SDS 1G 2G 3G NaCl 1G 2G 3G
B)
CTC-GNP
Std CE 1G 2G 3G
Std SDS 1G 2G 3G NaCl 1G 2G 3G
C)
ATC-GNP
Std CE 1G 2G 3G
Std SDS 1G 2G 3G NaCl 1G 2G 3G
250
150
100
75
50
37
25
20
15
10

Figure 6.